THE 25th GENERAL ASSEMBLY OF IASPEI
August 21 - September 1, 1989
Istanbul, Turkey

STRESS DROPS OF EARTHQUAKES IN AND NEAR THE MID-ATLANTIC RIDGE AS REVEALED FROM BODY-WAVE PULSE ANALYSIS

G-Akis Tselentis
Laboratory of Theor. and Appl. Seismology
Dept. of Appl. geology and Geophysics
The University of Patras
Patras 261 10
Greece

A B S T R A C T

To investigate the early tectonic processes of ocean lithosphere, we examine the stress drops of 11 earthquakes occurred in (7) and near (4) the Mid-Atlantic ridge.

The required parameters are derived from the azimuthal variation of body-wave pulse-widths through a least squares process, involving unilateral, bilateral and circular models of rupture propagation and various rupture velocities.

Combining this procedure with information obtained from long period body wave inversion, a more accurate evaluation of stress drops and other source properties was achieved and showed no systematic difference between the two types of events.

This is contribution No:10 of the laboratory of Theoretical and Applied Seismology of Patras University.

1. INTRODUCTION

Estimates of earthquake stress drops are important in the understanding of the regional stress field. Although a stress drop does not represent absolute levels of stress, it does indicate how much stress is being released during an earthquake, and therefore it gives a minimum value of the initial stress level.

Many studies of oceanic earthquakes have provided crucial information on the tectonics of oceanic regions. Normal faulting at mid-ocean ridges (Sykes 1967) identifies them as zones of active extension while in contrast, focal mechanisms in older ocean lithosphere indicate compressional stress, presumably due to "ridge push", the force caused by density inhomogeneities resulting from the thickening and subsidence of the cooling lithosphere (Bergman and Solomon 1980, Dahlen 1981).

Although the seismicity and source parameters of ridges and near ridge areas has been extensively studied, including analysis of body waves, surface waves and free oscillations there is little information about the involved stress drops. This is mainly due to the fact that most of the used techniques were applied in the frequency domain where only the amplitude spectrum is explained. One problem with estimating stress drops using the standard formula (e.g. Brune 1970) for a circular fault is the uncertainty introduced by the stress drop's cubic dependence on fault radius. Using Brune's model which assumes an infinite rupture velocity, one could obtain a fault radius from the corner frequency, or one could assume a more physically realistic model and try to estimate a rupture velocity and duration of the rupture. But accurate estimates of corner frequency are difficult to obtain from teleseismic waveforms because of the effect of scattering and attenuation.

On the other hand, the time domain approach permits both phase and amplitude spectra to be interpreted simultaneously and the theoretical prediction can be compared with the observation in a more direct way.

In the present investigation we are going to estimate earthquake stress drops from time domain information, through an inversion of azimuthal change in pulse width of body-waves, following a procedure similar to that of Chung (1979).

Since source dimensions and stress drops are usually model dependent (In particular estimated values for fault area and stress drop can vary substantially with different methods used), instead of assuming the same fault model for all events, several different models are being tested and compared and then the best one is used for the computations. To investigate any variations of stress drop it is desirable to compare stress drops determined by the same method. Thus, we can achieve a good estimate of relative stress drops even though the absolute values are to some extent model dependent.

2. METHOD OF ANALYSIS

During the present investigation, unilateral, bilateral and circular fault models are examined. For the first two models we assume that the rupture occurs simultaneously over the entire fault width and that the fault length is much larger than the fault width. Hence, the contribution from the fault width to the duration of the far field time function is assumed to be minor and can be neglected.

The waveforms of most of the analyzed earthquakes are relatively simple; the p-waves usually have a large first swing and a small second swing and then die away very quickly (Fig.1). The most important parameters characterizing the waveform are the pulse-width and the amplitude of the first swing, since the amplitude of the second swing can be compensated for, by choosing a proper shape for the far field source time function.

For the modes of rupture propagation shown in Fig.2, the duration of the far field source time function Ts can be expressed as (Chung 1979)

$$Ts = bX \qquad [1]$$

where

$$b = L/Vc \quad \text{(unilateral)}$$

$$= L/2Vc \quad \text{(bilateral)}$$

$$= a/Vc \quad \text{(circular)}$$

$$X = Vc/Vr - \cos\theta \quad \text{(unilateral)}$$

$$= Vc/Vr + |\cos 2\theta| \quad \text{(bilateral)}$$

$$= Vc/Vr + \sin\xi \quad \text{(circular)}$$

In the above equations, θ is the angle between the rupture direction and the ray taking off from point A to observation point P, and ξ (for circular model) is the angle between the normal to the fault plane and the ray taking off (Fig.2), Vc is the P- or S- wave velocity of the medium and Vr is the rupture velocity.

Having determined Ts at each individual station and for a given direction of fault propagation, the parameter θ can be calculated. Hence, the parameter b in equation [1] can be easily determined through a least squares approach. By repeating this procedure for each one of the three rupture models separately and for an accepted range of rupture velocities those parameters which give the minimum root-mean-square errors are adopted for further analysis.

To calculate the far field source time function S(t) from the recorded pulse R(t) on the records, we try to establish an analytical relation between the two, following the approach proposed by Chung (1979) but slightly modified since we perform

the calculations in the frequency domain. For this purpose we use a proper source time function and we take attenuation into account.

We can express R(t) as follows (Fig.1)

$$R(t)=S(t)*Q(t)*I(t) \qquad [2a]$$

or in the frequency domain

$$R(w)=S(w)Q(w)I(w) \qquad [2b]$$

where S(w) is the Fourier transform of the far field time function, I(w) the instrument response and Q(w) the earth's attenuation filter (Futterman 1962, Carpenter 1967), given by

$$Q(w)=\exp\{-wt^*+[iwt^*/(2\pi)]\ln[w/w')-2)\} \qquad [3]$$

with $t^*=\int ds/Q$, Q the quality factor and w' the Nyquist frequency. For P-waves from shallow teleseismic events t*=1 (Kanamori 1967), hence, by using various boxcar and triangular far field time functions we can easily establish a Ts versus Tr relationship

$$R(t)=\frac{1}{2\pi}\int_{-\infty}^{\infty} S(w)Q(w)I(w)\exp(-i2\pi wt)\,dw \qquad [4]$$

and by taking the average relation between the case corresponding to the boxcar and triangular functions we end up with a simple relation which is presented in graphical form in Fig.3 and is used to estimate the duration of the far field time function from the observed pulse-width on the seismic records.

During the analysis, we try to avoid multiple events and study earthquakes with relatively simple wave-forms. We are also restricted to earthquakes for which there are known fault plane solutions and seismic moments as obtained from the inversion of long period body waves. Seismic moments are usually well determined and not model dependent so we adopt the published values.

Assuming reasonable values for wave velocity Vc at the source depths we can calculate from the corresponding optimum b-values the fault dimensions. As far as the fault width is concerned, we assume that it equals 0.4 of the fault length (Ellsworth 1975). The obtained stress drops will be slightly different if a different width to length ratio is assumed and the relative stress drops do not change in any significant way.

For calculating the stress drops we employ the relation

$$\Delta\sigma=(7/16)Mo/(a^3) \qquad [5]$$

where a is the radius of the equivalent circular fault with area LW.

3. DATA ANALYSIS AND RESULTS

Eleven earthquakes near and in the Middle Atlantic ridge with depths less than 10Km and magnitudes ranging from 4.8 to 5.9 are investigated (Fig.4). We investigate earthquakes with known fault plane solutions and seismic moments, Table1, presents all the

relevant to the earthquakes information.

The duration of the first half swing of each event is measured from the long period WWSSN records at many stations (Fig.5), with close reference to the already published synthetic wave forms. The durations of the recorded half swings are then converted to the source duration by using the solid curve in Fig.3. Having the values of Ts at a number of stations the searching process described above is carried out through a series of least squares analyses for three different rupture modes. The rupture velocity is constrained within 0.4 to 0.9 of the shear wave velocity (Vs) and a fit is done for each increase of 0.1Vs. The processing scheme which was followed during the present analysis is illustrated in Fig.6.

The obtained results (Table2), shows that for the 11 events analyzed, unilateral rupture fits the observation best for 8 events, bilateral rupture gives best fits for 3 shocks and in no case does the circular faulting give the best fit. This inadequacy of the circular rupture mode to describe the rupture process can be explained as the effect of non isotropic material properties and stress field at the earthquake source region.

As shown in Table2, the source dimensions of the investigated earthquakes, vary from about 9.1 to 14.2Km with an average of about 12Km. The corresponding stress drops obtained vary from about 13.6 to 63.5 bars with a mean value of about 35 bars for the in ridge events and between 23 to 166 bars with an average of 71 bars for the off-ridge events.

It is known that the uncertainty in determining stress drops arises mainly from the uncertainty in the fault area. In the present investigation we have tried to reduce this uncertainty by first comparing several fault models with observations and then compute the fault area with the best model.

Chung (1979), pointed out that the fault length can be resolved to better than a factor of two for using the pulse-width technique. Assuming a factor of 1.5 for fault length resolution this results to a factor of 3 for stress.

The obtained stress drop values for the two examined categories of events show no systematic difference if one consider the error limits (presented as bars in Fig.7). On the other hand if we consider only average values there is a slight indication for the in ridge events to show relatively higher stress drops. This (if it is true), can be explained easy since stress drop is controlled by the temperature dependent material properties at the source region. However, the limited amount of examined data does not permit us to reach any conclusions and more earthquakes have to be analyzed.

4. SYNTHETIC SEISMOGRAMS

In order to test the quality of the obtained results, synthetic seismograms from the estimated source parameters are computed and then compared with the observations for a limited number of earthquakes. The method applied for the synthetics has been used for source studies of various events (Helmberger 1974, Chung and Kanamori 1976).

Basically, we model the far-field seismograms by convolving the

sum of various body wave rays (e.g. P, pP and sP) with source time history, earth attenuation, crustal structure and instrument response.

For the displacement of P waves we can write

$$Up(t)=Mo/(4\pi\rho_s V_{ps}^3)(g(\Delta,h)/a)R_{\theta\phi}^P S(t-T_s^P)*Q(t,Ts^P/Qav)*C(t)*I(t) \quad [6]$$

where

Mo= seismic moment
h = source depth
ρ_s = the density at source
V_{ps} = the wave velocity at source
a = earth's radius
$R_{\theta\phi}$= radiation pattern
and $g(\Delta,h)$ is the geometric spreading factor given by

$$g(\Delta)= \sqrt{\frac{\rho_n V_{ps}}{\rho_o V_o}\frac{\sin i_n}{\sin\Delta}\frac{1}{\cos i_o}\left|\frac{di_n}{d\Delta}\right|} \quad [7]$$

where ρ_o, V_{po}, i_o are the density, wave velocity and angle of incidence at the station respectively and ρ_n, V_{ps} and i_n are the same quantities at the source.

The crustal filter for a particular station can be written as

$$Co=[6\cos i\csc^2 i_o(1+3\cot^2 i)]/[4\cot i\cot g+(1+3\cot^2 i)^2] \quad [8]$$

with g the reflection angle of the SV waves which are generated by the reflection at the free surface.

During the calculation we assume trapezoidal far field functions S(t), whole rise times (t1s) are about 0.2 times the total duration Ts of the time function.

Fig.8 shows an example of comparison for event No1, we compare only the waveforms and not the absolute amplitudes. The theoretical seismograms are constructed assuming a source with a (unit) seismic moment of 10E25dyn-cm. Judging from Fig8, the obtained synthetics match the observed waveforms very well, suggesting that the results from pulse-width and least squares searching method are correct.

CONCLUSIONS

In this paper we have tried to compare stress drops between in ridge and near ridge earthquakes. We have tried to reduce the uncertainty concerning the estimation of fault area by first comparing several fault models with observations and then compute the fault area with the best model.

Despite the obtained small differences between the average stress drops for the two cases the limited amount of events investigated does not permit to reach any conclusion for the existence of a systematic difference in stress drops between the two kinds of events.

ACKNOWLEDGEMENTS

This project was carried out during my stay at the Earthquake Research Institute of Tokyo University. I thank K. Kudo and K. Chung for tutoring in the art of investigating earthquake source processes with waveform modeling and my colleagues at ERI for stimulating conversations. Repeated use of the film chip collection at ERI is gratefully acknowledged.The research was partially supported by a grant from the Directorate of Research and Development of the European Communities.

REFERENCES

Bergman, E. A., and Solomon, S.C., 1980. Oceanic intraplate earthquakes: Implications for local and regional intraplate stress. J. Geophys.Res., 85, 5389-5410.

Brune, J.N., 1970. Tectonic stress and spectra of seismic shear waves from earthquakes. J. Geophys. Res., 75, 4997-5009.

Carpenter, E.W., 1967. Teleseismic signals calculated for underground, underwater, and atmospheric explosions. Geophysics XXXII, No1,17-32.

Chung, W.Y., 1979. PART I: Variation of seismic source parameters and stress drop within a descending slab as revealed from body-wave pulse-width and amplitude. Ph.D Diss., California Institute of Technology, 93pp.

Dahlen, F.A., 1981. Isostasy and the ambient state of stress in the oceanic lithosphere. J. Geophys. Res., 86,7801-7807.

Ellsworth, W.L., 1975. Bear Valley, California, earthquake sequence of February-March, 1972. Bull. Seism. Soc. Am., 65, 483-506.

Futterman, W.I., 1962. Dispersive body waves. J. Geophys. Res.67, 5279-5291.

Helmberger, T., 1974. Generalized ray theory for shear dislocation. Bull. Seism. Soc. Am., 64, 45-64.

Kanamori, H., 1976. Re-examination of the Earth's free oscillations excited by the Kamchatka earthquake of November 4,1952. Physics of the Earth and Planetary Interiors 11, 216-226.

Sykes, L.R., 1967. Mechanism of earthquakes and nature of faulting on the mid-oceanic ridges. J. Geophys.Res., 72, 2131-2153.

CAPTIONS OF TABLES

TABLE 1: Earthquakes used in the present analysis

TABLE 2: Source parameters

CAPTIONS OF FIGURES

FIG.1: Calculation of theoretical pulse-width Tr on a seismic record R(t) by convolving a boxcar far field tme function S(t) with a Q-filter Q(t) and an instrument impulse response I(t).

FIG.2: Modes of rupture propagation considered in the present research.

FIG.3: Relationship between the far field source time function duration (Ts) and pulse width duration of a seismic record (Tr).

FIG.4: Epicentral location of the 11 near-ridge and in-ridge earthquakes used.

FIG.5: Focal mechanisms and used P-waves for the 11 events.

FIG.6: Processing scheme used in the present analysis.

FIG.7: RMS errors for the three rupture modes.

FIG.8: Comparison between the synthetic (dashed curves) and observed (solid curves) seismograms of earthquake number 1 at three stations.

TABLE 1

No	DATE	LAT(N)	LONG(E)	MAGN(m)	MOMENT(10dyn-cm)
	NEAR RIDGE EVENTS				
1	Aug.6 62	32.26	-41.03	5.6	13
2	Aug.8 69	-47.76	-15.66	5.7	15
3	Jul.1 74	-22.57	-10.68	5.5	3.3
4	Sep.13 81	24.87	-46.30	5.8	8.9
	IN RIDGE EVENTS				
5	Sep.20 69	58.35	32.08	5.6	15
6	Apr.3 72	54.33	35.20	5.1	4.4
7	Jun.28 77	22.64	45.07	5.3	3.0
8	Apr.22 79	33.00	39.72	5.6	9.9
9	Jun.28 79	00.40	24.96	5.5	3.6
10	Jun.6 72	32.93	39.79	5.3	4.1
11	May.12 83	17.63	46.53	5.7	7.1

TABLE 2

No	STANDARD ERROR OF ESTIMATE			Vr/Vs	LENGTH	AREA	STRESS-DROP
	Unilat.	Bilat.	Circular		(Km)	(Km^2)	Bar
1	0.637	0.732	0.801	0.8	9.1	33.1	166
2	0.793	0.656	0.991	0.9	14.2	80.3	51
3	0.679	0.809	1.001	0.9	11.1	49.5	23
4	0.931	0.956	1.017	0.8	12.6	63.5	43
5	0.433	0.502	0.516	0.9	13.2	69.3	63
6	0.920	0.953	0.972	0.9	10.8	42.6	34
7	1.571	1.432	1.593	0.7	12.8	66.1	14
8	0.529	0.546	0.531	0.9	13.5	72.9	39
9	0.796	0.632	0.723	0.8	10.5	44.1	30
10	0.841	0.875	0.879	0.9	12.5	62.3	20
11	0.646	0.696	0.782	0.9	11.5	52.6	45

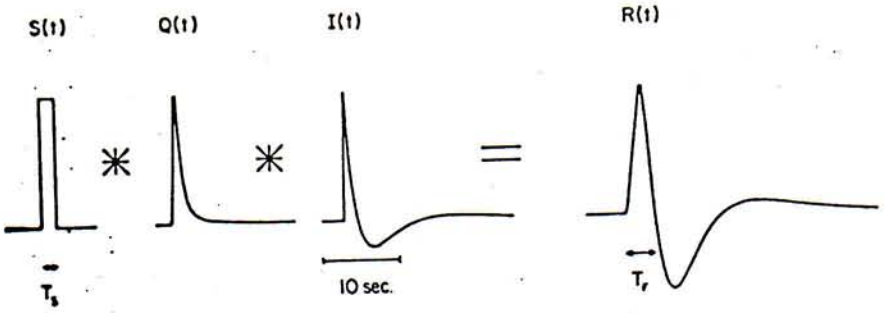
S(t)
Q(t)
I(t)
R(t)
T_s
10 sec.
T_r

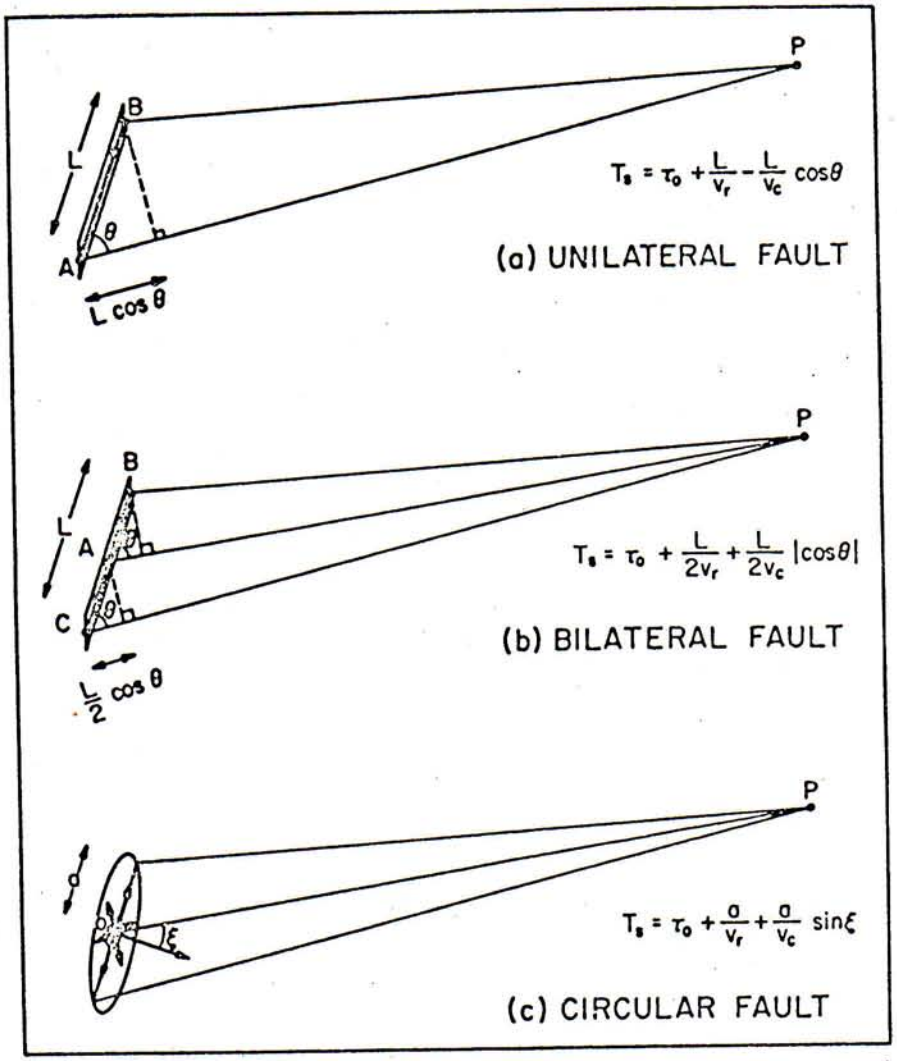
P
B
L
θ
A
L cos θ
$T_s = \tau_0 + \frac{L}{v_r} - \frac{L}{v_c}\cos\theta$
(a) UNILATERAL FAULT
P
B
L
A
C
θ
$\frac{L}{2}\cos\theta$
$T_s = \tau_0 + \frac{L}{2v_r} + \frac{L}{2v_c}|\cos\theta|$
(b) BILATERAL FAULT
P
a
ξ
$T_s = \tau_0 + \frac{a}{v_r} + \frac{a}{v_c}\sin\xi$
(c) CIRCULAR FAULT

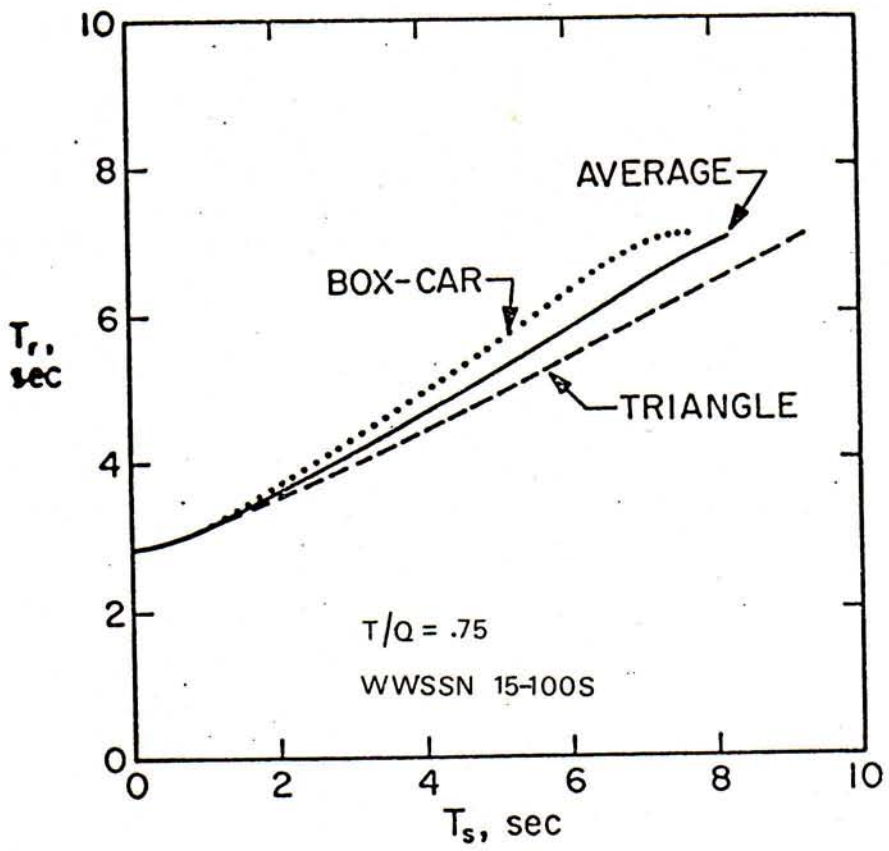
10
8
6
4
2
0
0
2
4
6
8
10
AVERAGE
BOX-CAR
TRIANGLE
T/Q = .75
WWSSN 15-100S
T_r, sec
T_s, sec

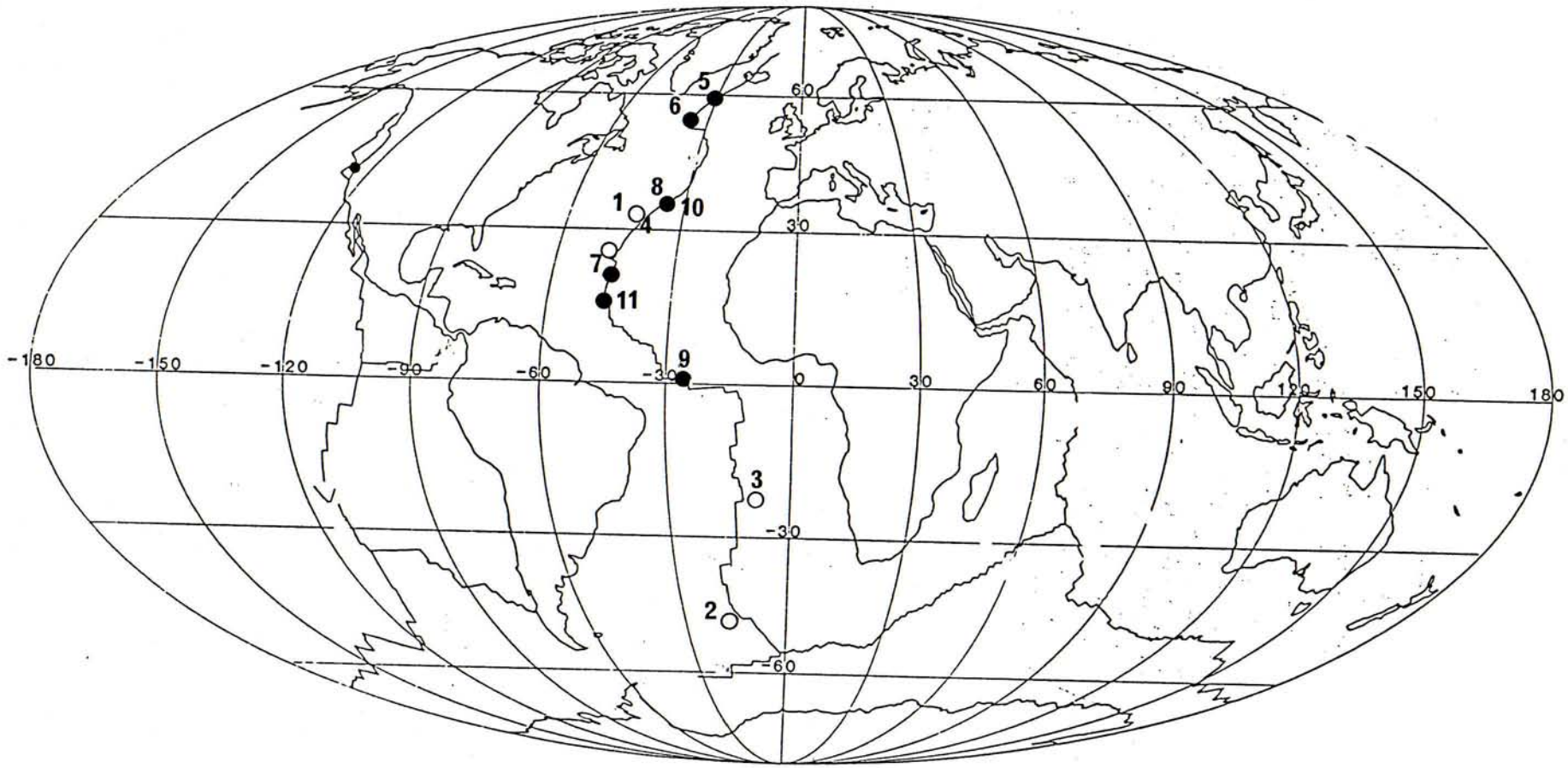
1
2
3
4
5
6
7
8
9
10
11
60
30
-30
-60
-180
-150
-120
-90
-60
-30
0
30
60
90
120
150
180

P WAVES

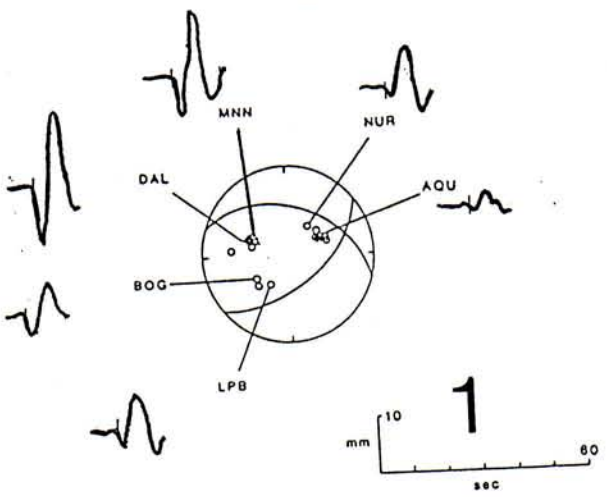
MNN
NUR
DAL
AQU
BOG
LPB
10
mm
60
sec
1

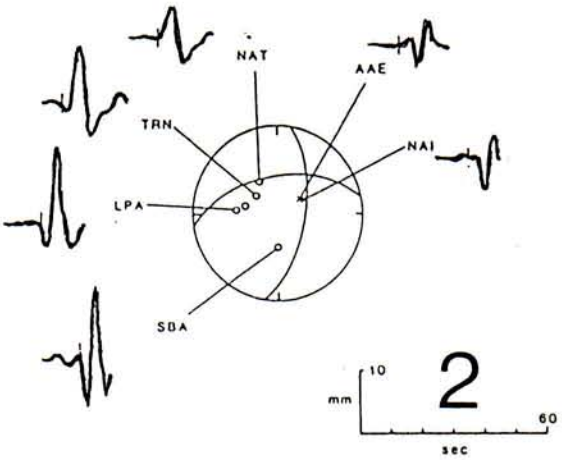
NAT
AAE
TRN
NAI
LPA
SBA
10
mm
60
sec
2

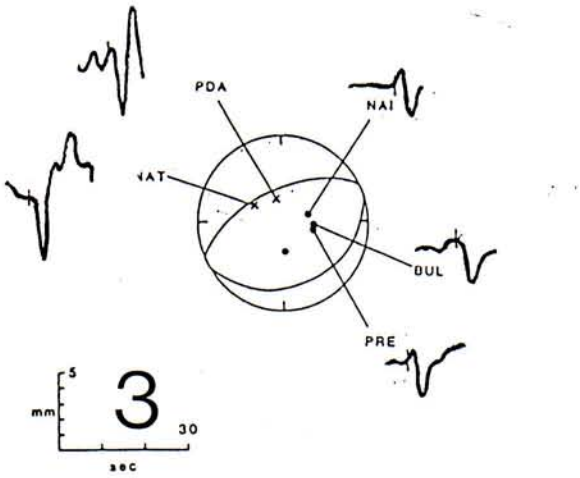
PDA
NAI
NAT
DUL
PRE
5
mm
30
sec
3

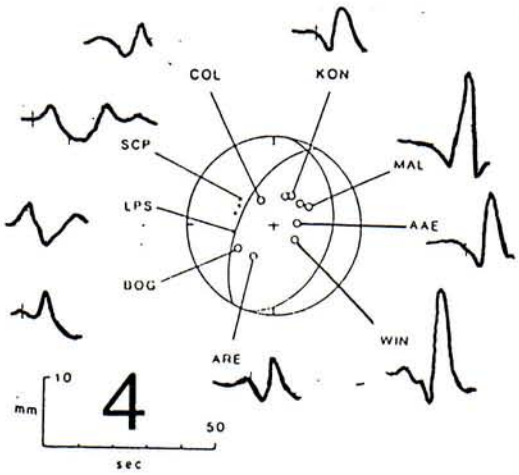
COL
KON
SCP
MAL
LPS
AAE
DOG
ARE
WIN
10
mm
50
sec
4

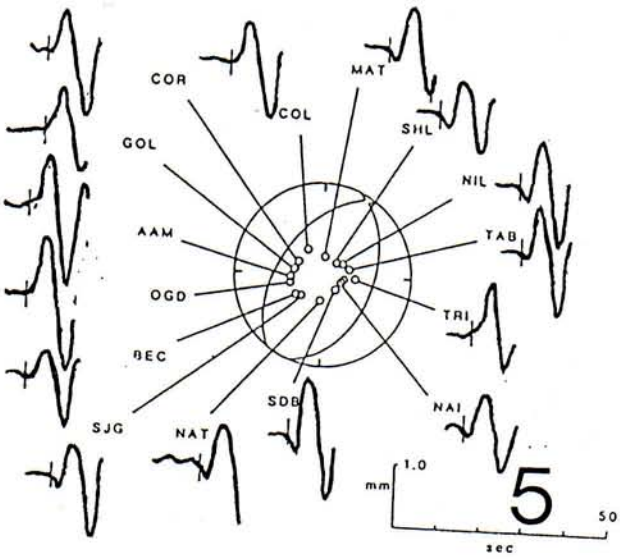
COR
COL
MAT
SHL
GOL
NIL
AAM
TAB
OGD
TRI
BEC
SJG
NAT
SDB
NAI
1.0
mm
50
sec
5

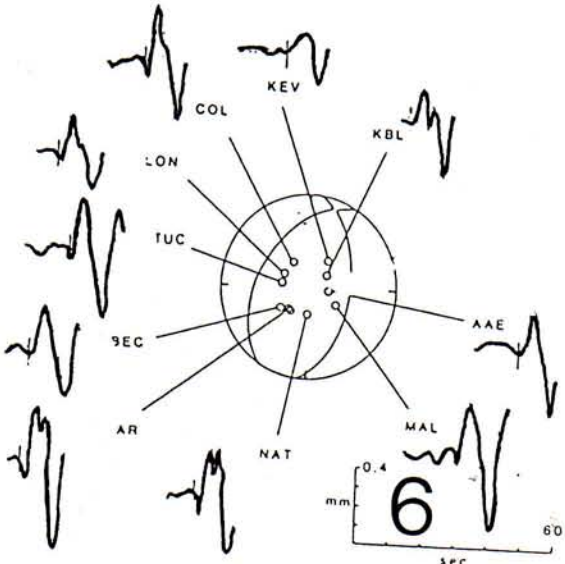
KEV
COL
KBL
KON
TUC
BEC
AAE
AR
NAT
MAL
0.4
mm
60
sec
6

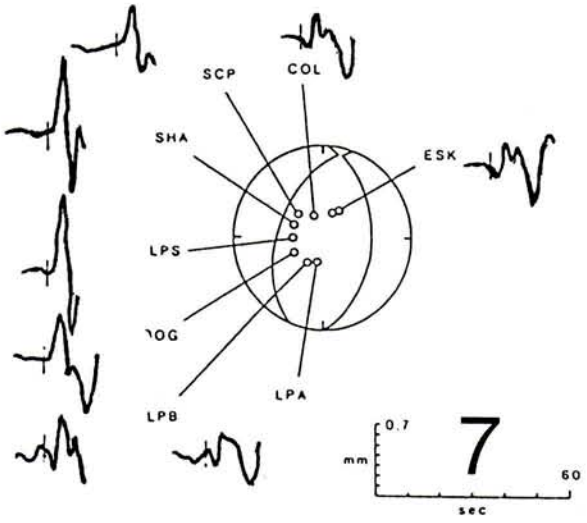
SCP
COL
SHA
ESK
LPS
LPA
LPB
0.7
mm
7
60
sec

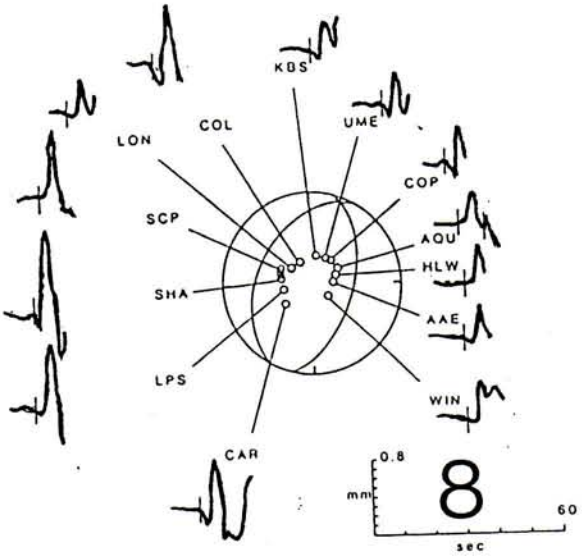
KBS
LON
COL
UME
COP
SCP
AQU
SHA
HLW
AAE
LPS
WIN
CAR
0.8
mm
8
60
sec

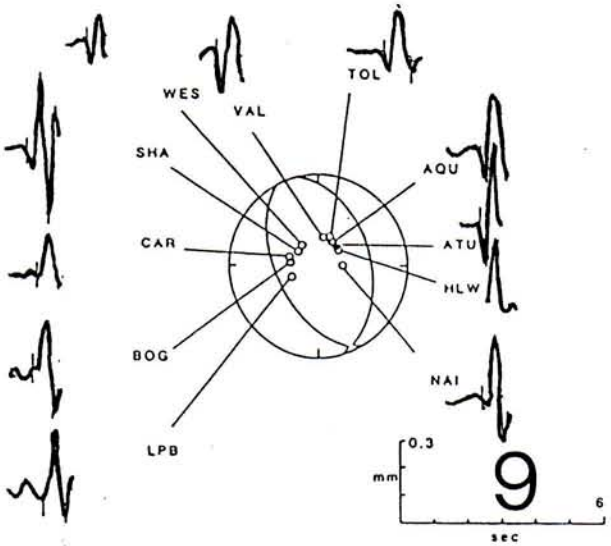
WES
TOL
VAL
SHA
AQU
CAR
ATU
HLW
BOG
NAI
LPB
0.3
mm
9
6
sec

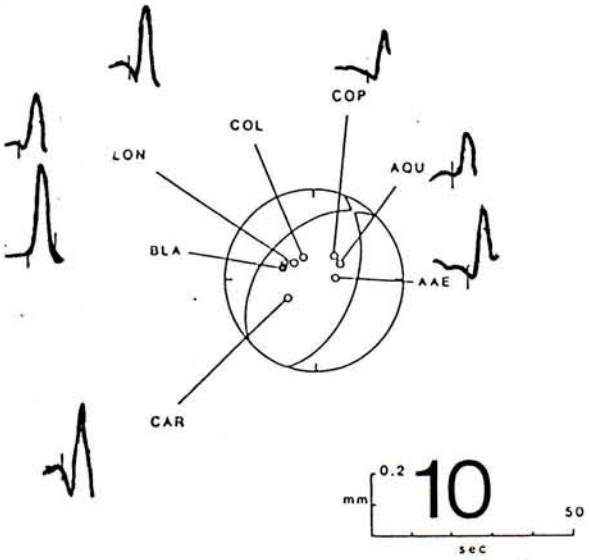
COP
COL
LON
AQU
BLA
AAE
CAR
0.2
mm
10
50
sec

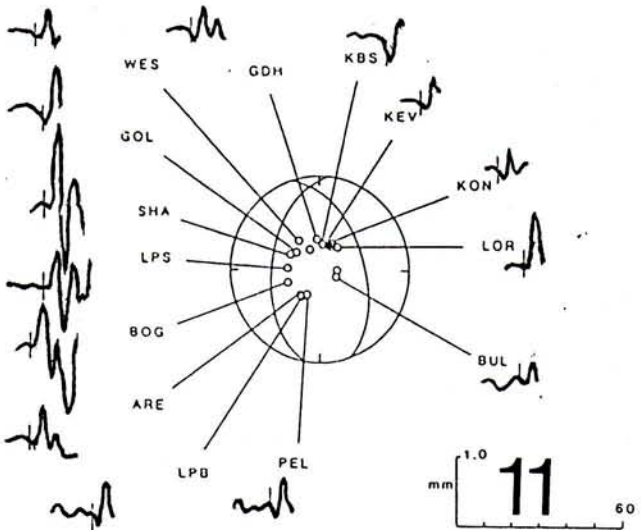
WES
GDH
KBS
KEV
GOL
KON
SHA
LOR
LPS
BOG
BUL
ARE
LPB
PEL
1.0
mm
11
60

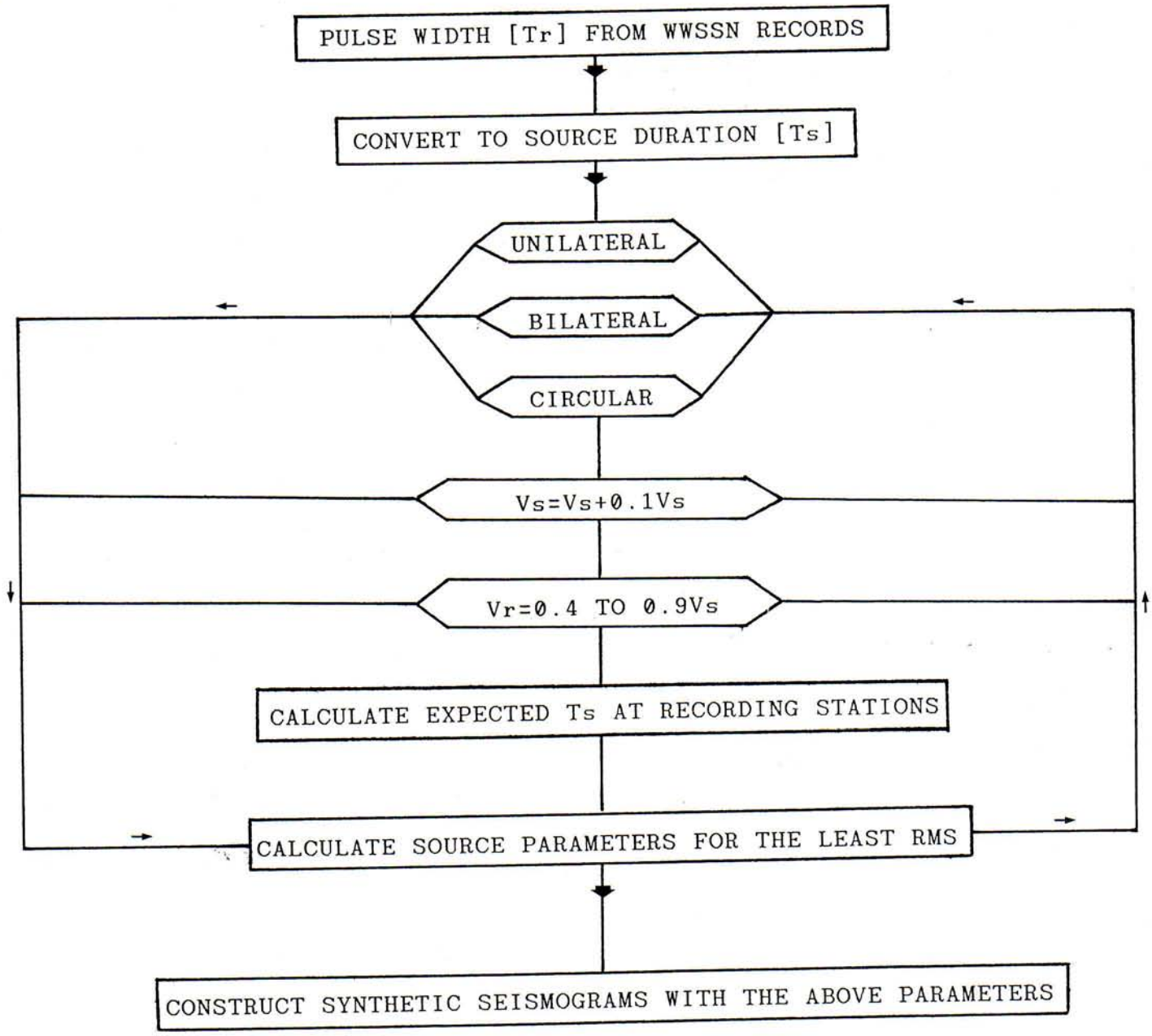
PULSE WIDTH [Tr] FROM WWSSN RECORDS
CONVERT TO SOURCE DURATION [Ts]
UNILATERAL
BILATERAL
CIRCULAR
Vs=Vs+0.1Vs
Vr=0.4 TO 0.9Vs
CALCULATE EXPECTED Ts AT RECORDING STATIONS
CALCULATE SOURCE PARAMETERS FOR THE LEAST RMS
CONSTRUCT SYNTHETIC SEISMOGRAMS WITH THE ABOVE PARAMETERS

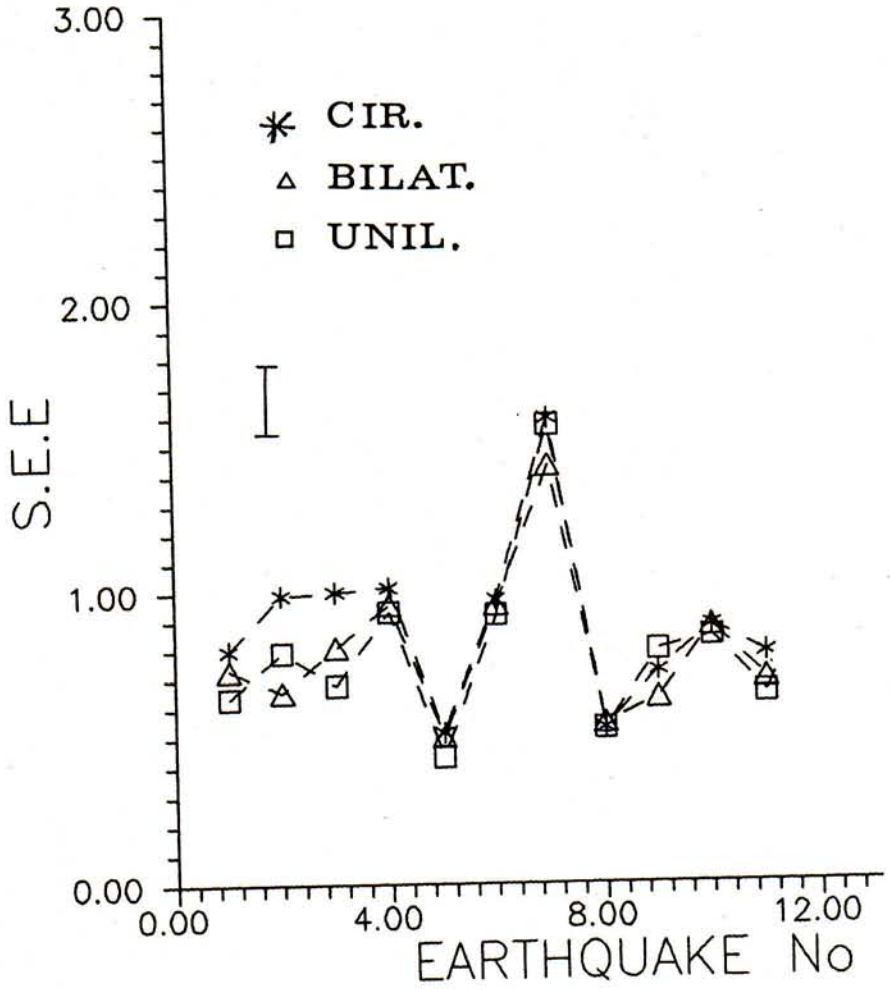
3.00
2.00
1.00
0.00
S.E.E
CIR.
BILAT.
UNIL.
0.00
4.00
8.00
12.00
EARTHQUAKE No

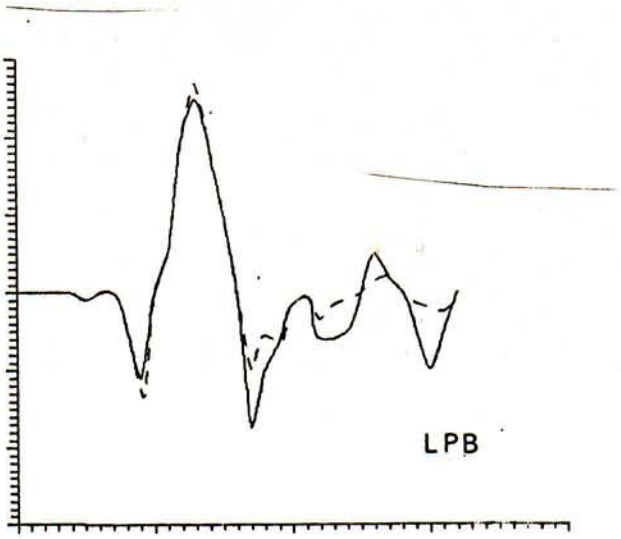
LPB

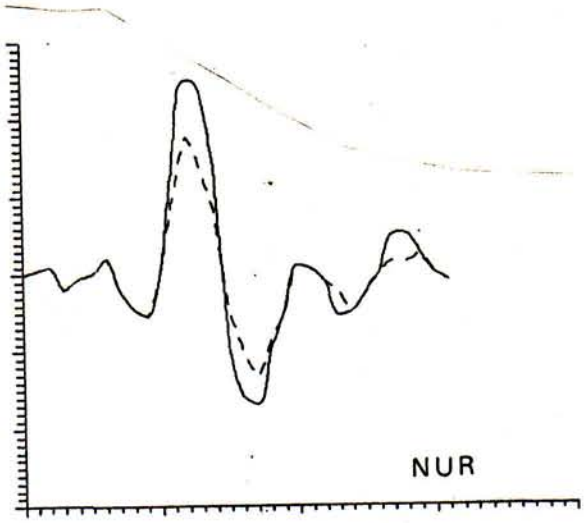
NUR

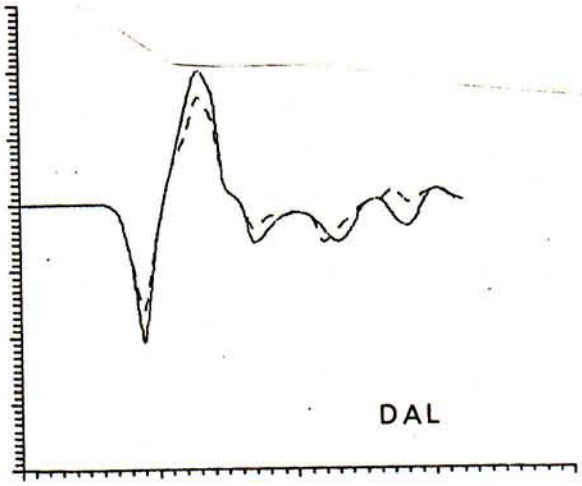
DAL